ADVANCED MATERIALS INTERFACES
www.advmatinterfaces.de

3D-Printed Cactus-Inspired Spine Structures for Highly Efficient Water Collection

*Xiangjia Li, Yang Yang, Luyang Liu, Yiyu Chen, Ming Chu, Haofan Sun, Weitong Shan, and Yong Chen**

The inherent fog collection mechanism used by the cactus gives inspirations for constructing energy-efficient and environmentally friendly water collection devices. However, the related studies meet the bottleneck on improving the collection efficiency because it is hard to replicate real natural clusters of branched spines by traditional manufacturing methods. The immersed surface accumulation based 3D printing provides a tool to reproduce branched cactus spines, enabling the study of water collection of artificial spines with various designs. Here, a cactus-inspired surface decorated with multiple directional artificial spines for highly efficient water collection and transportation is presented. The nanoscale hydrophobic coating is sputtered on the surface of the 3D-printed spines to accelerate the water growth rate. The results show that the hexagonally arranged clusters enhance the moisture airflow around 3D-printed spines, and the printed spines with 10° tip angle and hydrophobic coating achieve the highest weight gain of 2 mg min^{-1} mm^{-3}. This study opens intriguing perspectives for designing next-generation structural materials with the special spatial distribution of biomimetic features to achieve energy free and highly efficient water collection. The results reported here are believed to be helpful for the development of environmental friendly water collection, water transportation, and water separation devices.

1. Introduction

The risk of water shortages worldwide is becoming a serious issue in recent decades. The water crisis results from the insufficiency of the total water mass and the inadequacy of water collection and preservation in those regions.[1] Fog collection has been attracting much attention due to its large water capacity and the emergence of the worldwide water crisis.[2–6] Biological constructs comprise a significant source of inspiration for the design of next-generation structural materials since the creatures in nature possess almost perfect structures and functions after millions of years of evolution. For example, Namibia Desert beetles and spider silks can efficiently collect water from the fog.[4,7] Many members of the Cactaceae family can survive in highly arid deserts by using spines that collect fog from multiple directions.[8–14] The gradient of surface-free energy and gradient of Laplace pressure are the primary driving forces behind these phenomena.[15–19] Various kinds of bioinspired fog collectors based on different surface wettability have been proposed.[20–23] Some of the fog collectors depend on gravitational or other external forces to transport or remove the collected water. But the large size required for water drops to move on the solid surface by gravity hinders the rebirth of the fog collection cycle.[24] Inspired by the spider silk and cactus to address this problem, others used gradient surfaces for efficient and continuous fog collection

Dr. X. Li, Dr. Y. Yang, Prof. Y. Chen
Epstein Department of Industrial and Systems Engineering
University of Southern California
3715 McClintock Ave, Los Angeles, CA 90089, USA
E-mail: yongchen@usc.edu
Dr. X. Li
School for Engineering of Matter, Transport and Energy
Arizona State University
551 E Tyler Mall, Tempe, AZ 85281, USA
Dr. Y. Yang
Department of Mechanical Engineering
San Diego State University
5500 Campanile Drive, San Diego, CA 92182, USA
L. Liu, M. Chu, H. Sun, W. Shan
Mork Family Department of Chemical Engineering and Material Science
Viterbi School of Engineering
University of Southern California
925 Bloom Walk, Los Angeles, CA 90089, USA
Y. Chen, Prof. Y. Chen
Department of Aerospace and Mechanical Engineering
Viterbi School of Engineering
University of Southern California
854 Downey Way, Los Angeles, CA 90089, USA
The ORCID identification number(s) for the author(s) of this article can be found under https://doi.org/10.1002/admi.201901752.

DOI: 10.1002/admi.201901752

by the Laplace pressure gradient arising from the shape and the wettability gradient.[4,5,15,17,25–28] For example, many kinds of dual-gradient 1D fog collectors have been studied.[24–26] Recently, cactus spine-like conical microtips have been fabricated by chemical or electrochemical erosion of metal wire,[17] deep X-ray etching,[29] replica molding method,[30–32] etc. Although these reported methods can successfully prepare well-defined conical microtips and their arrays, most of them are focused on the study of single spine arrays, while natural cactus possesses multispines with highly efficient fog collection. The fabrication of multispines arrays with controllable arrangement as in nature is challenging.[33] The branched spine arrays with the controllable 3D geometric shape that can dramatically increase fog collection efficiency are hard to fabricate by the traditional methods.[34,35]

Additive manufacturing (aka 3D printing) is one of the effective ways of fabricating customized parts with complicated architectures and has wide applications in industry, academia, and daily usages.[36] 3D printing presents a new direction for the fabrication of complex bioinspired structures in nature.[37–41] Here, we presented a 3D-printed water collector with microscale biomimetic branched spines with controllable spine tip angle and wettability to improve the water collection efficiency. The composite material was developed and postprocessed to modify the wettability of the 3D-printed spines for better performance. The arrangement of the branched spines was further studied and optimized based on the theory of aerodynamics. The hexagonally arranged branched spines showed promising properties in terms of water collection and transportation. As environmentally friendly structures with no external energy, the new 3D-printed surface with the optimized biomimetic multibranched spines has prospective applications in energy-efficient water collection, water transportation, and oil–water separation.[42]

2. Results and Discussion

Cactus was discovered to be able to collect water continuously and efficiently by using its clusters of conical spines and belt-structured trichomes on the succulent stems.[5,43] Micronized water drops collected can be transported directionally away from the original deposition site under the gradient of Laplace pressure as soon as they grow to a critical size on the conical arrays.[4,44,45] This quick regeneration of the deposition sites guarantees efficient fog collection. A typical cactus stem is shown in **Figure 1**a. Clusters of spines are distributed evenly on the stem, and each spine has an apex angle 2α around 10° (Figure 1a). The spines in various directions guarantee the water collection efficiency from different directions of fog flows

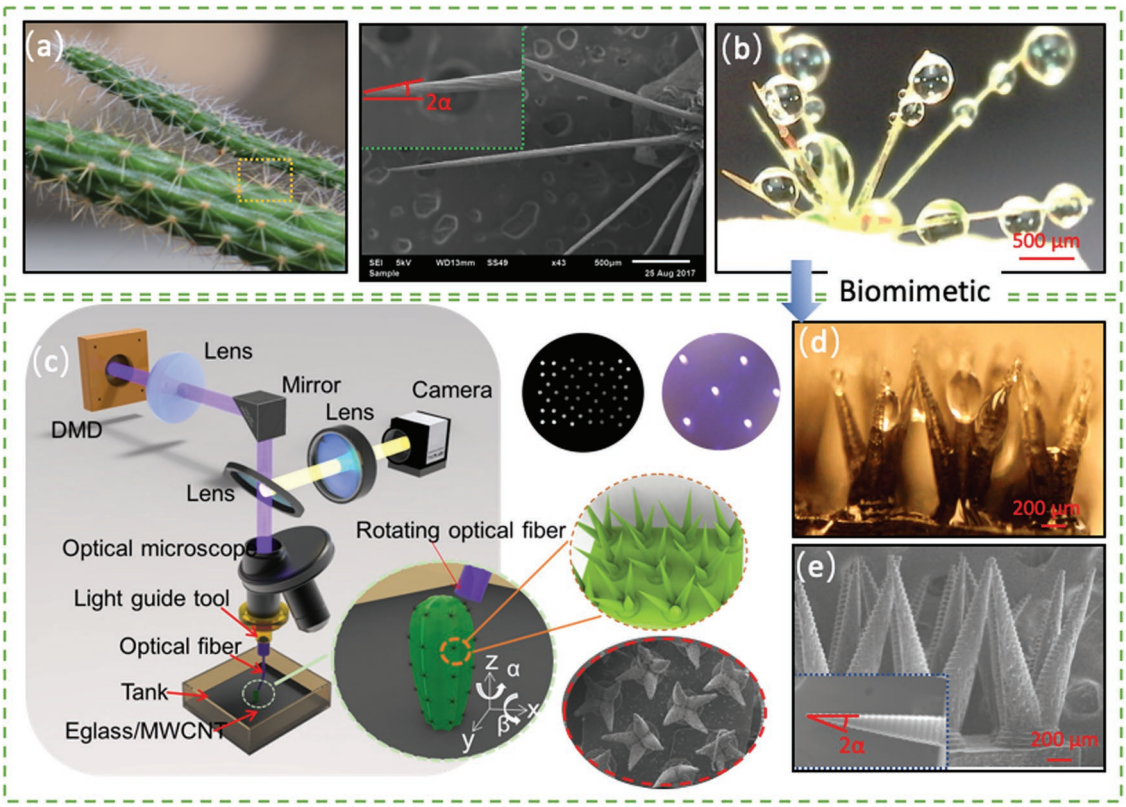

Figure 1. Biomimetic water collection structure: a) natural cactus with the scanning electron microscope (SEM) images showing b) the spines and water collection capability; c) schematic diagram of the ISA-based 3D printing (ISA-3DP) process; the optical system in the ISA-3DP process (inset shows the magnification of the light guide tool and the optical fiber with projected 2D micropatterns) with the designed models; d) the water collection capability and e) the SEM image of the 3D-printed cactus-mimetic spine arrays.

(Figure 1b). However, the collected water is not easy to transport from the top tip to the base for the cactus spine (Movie S1, Supporting Information). Inspired by the principle of multiple spines' water collection capability, we digitally designed the artificial spine arrays in different arrangements and fabricated them using 3D printing to speed up the water collection and transportation. In our developed 3D printing process, a set of conical spines with tip angles ranging from 10°, 20°, 30°, 40° to 50° were obtained (see the Experimental Section). The water collection ability of the 3D-printed spine arrays was investigated under a saturated water flow with relative 95% humidity at room temperature. The layer-based immersed surface accumulation 3D printing (ISA-3DP) process, enabling one to build microscale biomimetic structures around an inserted object was applied to fabricate artificial multibranched spines (Figure 1c).[38,46] The stair-stepping effect was generated due to the layer-by-layer accumulation of the material. Such stair-stepping effect is beneficial since, besides the top tips of spines, the water droplets were collected at the corners of neighboring stairs due to the curvatures change, enabling more water collection compared with the smooth surface (Figure S2, Supporting Information). In ISA-3DP, the light guide tool, consisting of an optical rod and an objective lens, was inserted inside the resin tank filled with photocurable liquid resin (E-glass/multiwall carbon nanotubes (MWCNTs)). The 2D patterned light beams were focused on the top surface of the light guide tool, and a series of mask images were projected in a sequence along with the movement of the light guide tool. Under the illumination of the 2D patterned light beam, the photocurable composite resin was selectively cured into solid. The 3D-printed artificial spines were flexible, and the shape of 3D-printed spines recovered after they bent under compression load no larger than 6 N (Figure S4, Supporting Information). The recovered 3D-printed artificial spines still showed similar water collection capability. An array of the 3D-printed multibranched spines with 10 apex angle was designed as shown in Figure 1e. When it was put in the same environment where the natural cactus spines were put (refer to Figure 1b), the water droplet grew on each 3D-printed spines (Figure 1d).

Digital models of multibranched spines array with different tip angles and arrangements were created using Solidworks, and each model was sliced into a series of 2D pattern images, of which the layer thickness was equal to 35 μm (**Figure 2**a). The light intensity of projection beam generated by our optical system was calibrated, and the grayscale level of each pixel in the 2D patterned mask images was adjusted to achieve uniform light intensity distribution (Figure 2b). Cluster arrays with different numbers of cactus-mimetic branched spines (N = 1–4) were designed and fabricated using ISA-3DP to study the water collection efficiency of different cactus-inspired microstructures (refer to Figure 2c–f). To generate the sharp tip of the artificial spine of which the dimension was smaller than 8 μm, the exposure time of each layer was set based on the dimension of the projected 2D patterned light beam (Figure S1, Supporting Information).[46] The layer-based ISA-3DP process to fabricate the artificial spine array can increase the surface roughness, which can help the water droplet growth at different places along the printed artificial spine (Movies S1–S3, Supporting Information). After curing one layer of material, the previously cured layers moved away from the light guide tool, and the distance between the light guide tool and the previously cured layers was maintained at 35 μm to ensure the following layer to stick onto the previously built layers. To prohibit the over cure features in the fabrication direction, the cure-depth of liquid resin was controlled by adding MWCNTs or Oil Red O dye.[38,46]

The water collection performance of the artificial spine is determined by its shape, wettability, and arrangement, and the water collection efficiency of cactus-mimetic spines is related to its water condensation rate and water transportation speed.[47] The water condensation is determined by the vapor pressure of water. The water droplet begins to grow rapidly when the embryo exceeds the critical size r_c and the vapor pressure is below the actual pressure.[48] The vapor pressure of water can be calculated based on Kelvin equation[48]

$$P = e^{\frac{2\sigma_w V_{ml}}{RT}\kappa} P_s \tag{1}$$

where V_{ml} is the molar volume of water, σ_w is the surface tension of water, R is gas constant, T is the temperature, P_s is the saturated vapor pressure of water on a flat surface, and P is the vapor pressure of water on a surface with curvature κ.

The critical coagulate radius r_c of water can be defined as follows

$$r_c = \frac{2\sigma_w V_{ml}}{RT \ln\left(\frac{P}{P_s}\right)} \tag{2}$$

The vapor pressure was increased with the increase of curvature κ of the cactus-mimetic spine tip. The water collection of the 3D-printed spines was studied by adjusting the tip angle of the cactus-mimetic spine. It was noticed that water droplets can be obviously observed on the tip of the cactus-mimetic spines with 10°, but there was no significant water droplet growth on the tip of the spines with 50° (**Figure 3**a) after 1 min. The water droplet growth speed of the 3D-printed spines with 10° is much faster than the one designed with larger tip angles at each time. As shown in Figure 3b, the water collection weight gain of cactus-mimetic spines with 10° is 1.5 times of the one designed with 50° at the same time, and is five times of the flat surface without spines. Hence, water vapor coagulation is easier to occur at the place of the 3D-printed spines designed with a high radius of curvature. However, the strength of the 3D-printed spines would be weaker with the decrease of the tip angles.

Meanwhile, the critical radius of water can be reduced by lowering the surface tension. The surface tension of the hydrophobic surface is smaller than the hydrophilic surface. Based on Equation (2), the critical coagulate size of the water droplet on the hydrophobic surface is smaller compared with the hydrophilic surface. Thus, the condensation of the water droplet is easier to occur on the hydrophobic surface than hydrophilic surface under the same conditions.[49,50] The nanocomposite material (E-glass with MWCNTs) shows hydrophilic behavior (Figure S3a, Supporting Information). Its surface wettability was modified by coating nanoscale superhydrophobic layer.[51] Note the superhydrophobicity was enhanced by adding MWCNT due to the increasing roughness (Figure S3d–f, Supporting

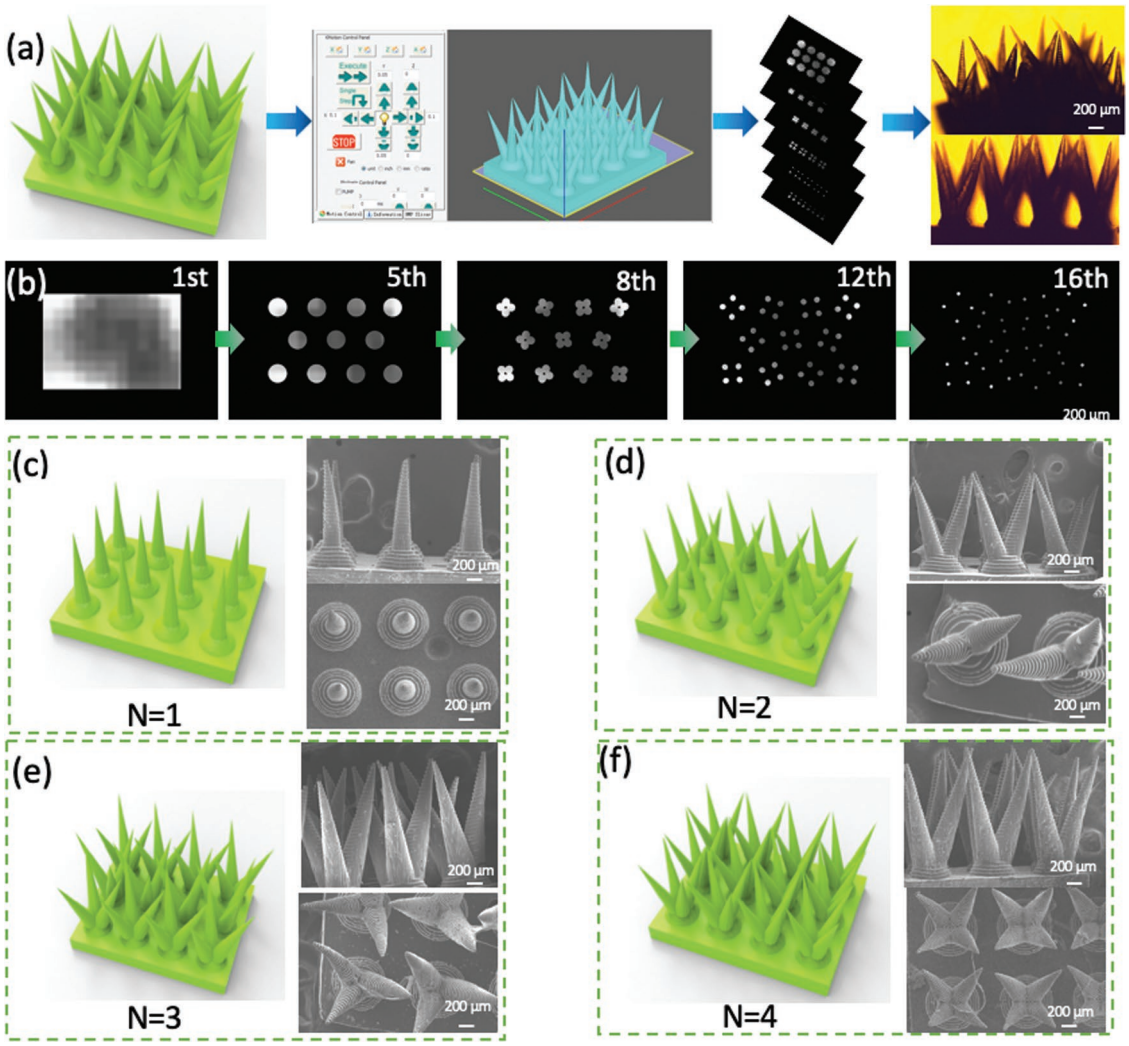

Figure 2. Schematic diagram of the fabrication process of various cactus-mimetic structures by the ISA-3DP process. a) A spines array model designed using Solidworks, sliced in our digital micromirror device based stereolithography (DMD-based SL) software, and the optical microscopy images of the 3D-printed spine array; b) the sliced images of different layers for the printing of cactus-mimetic arrays with $N = 4$; and c–e) the SEM images of the 3D-printed cactus-mimetic arrays with different number of spines: $N = 1$, $N = 2$, $N = 3$, and $N = 4$.

Information). After sputtering the superhydrophobic coating, the contact angle of water on the flat surface was increased from 65° to 137° (Figure S3b,c, Supporting Information). The drawbacks of the water collectors without the sputter coating is that the critical coagulate radius of water for the condensation is large and more time is required to collect the same amount of water. In addition, the delayed surface refreshment further counts against efficient water collection.[45] After the sputtering of superhydrophobic nanomaterial, the outer surface of the 3D-printed artificial spine becomes superhydrophobic, and the water droplet was easily formed that can be released on time. As a result, the water droplet grew faster on the 3D-printed cactus-mimetic spines with coating than the one without coating at each time (Figure S3g, Supporting Information). The water collection rate of nanocomposite-based cactus-mimetic spines with superhydrophobic coating was nine times than that of the 3D-printed polymer-based spines without coating (Figure S3h, Supporting Information).

To continuously collect water on the tip of the 3D-printed spines, the condensed water droplet needs to move along the cactus-mimetic spines to the base. The spines' directions of growth from the cactus stem were not apparently a key factor in the directional movement of the water drops. The water transportation of cactus-mimetic spines is attributed to the Laplace pressure difference at two sides. The pressure difference can be represented by the following formula[17]

$$\Delta P_{\text{curvature}} = -\int_0^{L^*\tan\frac{\alpha}{2}} \frac{2\sigma_w}{(R+R_0)^2}\sin\frac{\alpha}{2}\,\mathrm{d}z \tag{3}$$

where $\Delta P_{\text{curvature}}$ is the gradient of Laplace pressure, L is the height of 3D-printed cactus-mimetic spine, and R_0 is the radii of the 3D-printed cactus-mimetic spine and the collected water droplet, α is the tip angle of the 3D-printed cactus-mimetic spine, and $\mathrm{d}z$ is the integral variable of the 3D-printed cactus-mimetic spine.

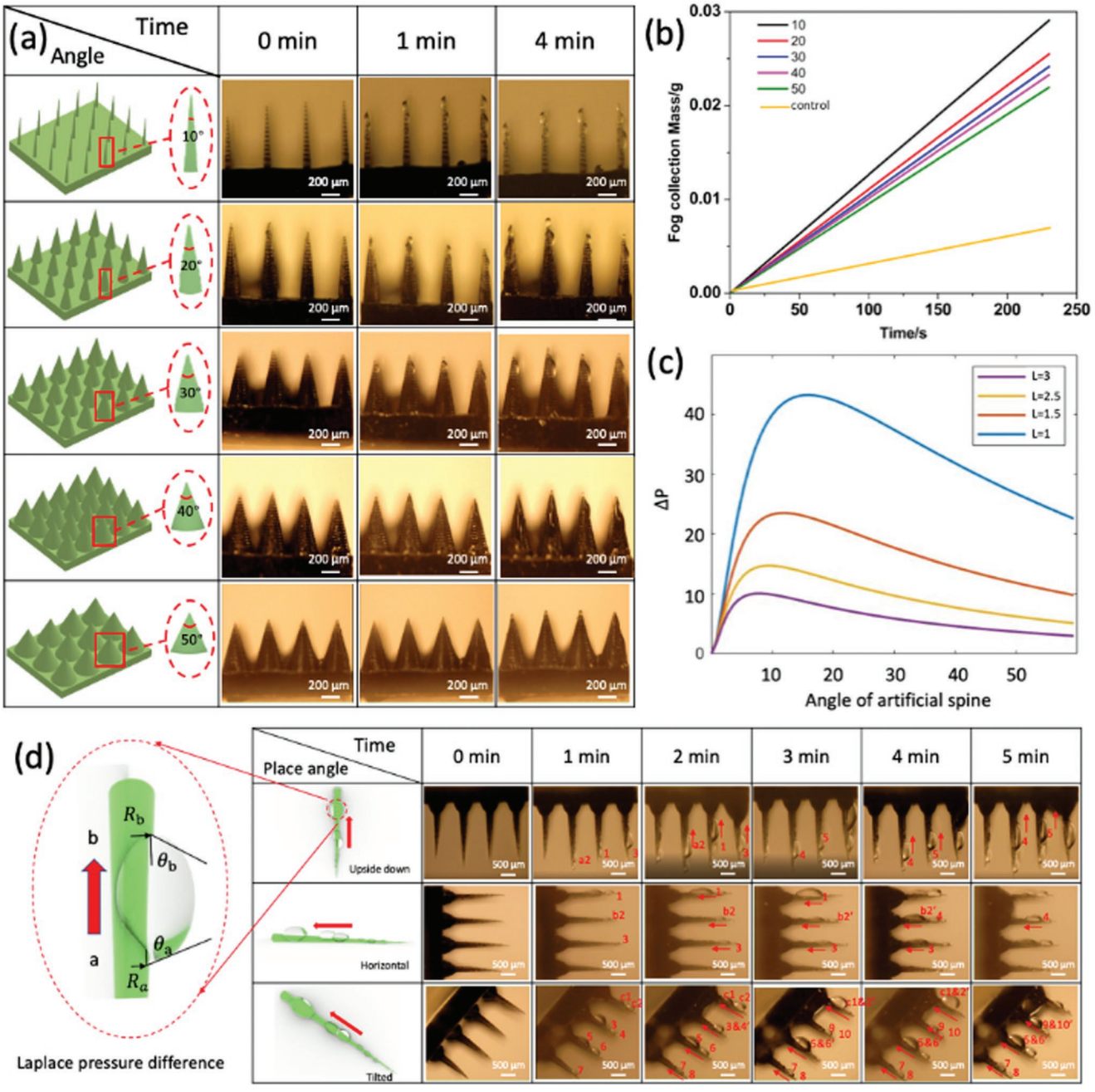

Figure 3. Water condensation and transportation of the 3D-printed cactus-mimetic spine structures. a) The microscope images of the water collection process over time for the spines designed with different tip angles at 0, 1, and 4 min; b) the collected water masses of the surface decorated with and without spines designed with different tip angles with time; c) the Laplace pressure difference for the spines designed with different tip angles and lengths; and d) the water transportation along the 3D-printed cactus-mimetic spine structures placed at different tilting angles.

The pressure difference, which promotes the condensed water droplet to move from the tip to the base, is determined by the tip angle and the height of the 3D-printed cactus-mimetic spine

$$\Delta P_{\text{curvature}} = \frac{2\sigma_w \sin\frac{\alpha}{2}}{\left[(L-2R_0)\tan\frac{\alpha}{2}+R_0\right]^2} - \frac{2\sigma_w \sin\frac{\alpha}{2}}{\left(L\tan\frac{\alpha}{2}+R_0\right)^2} \quad (4)$$

For the fixed height, the pressure was firstly increased dramatically to the peak value and then reduced with the increment of the tip angle. From the observation of the simulation curve shown in Figure 3c, the optimal tip angle of 3D-printed cactus-mimetic spines turned to be smaller with the increase of its height for fast water transportation. The 3D-printed cactus-mimetic spines achieved fast water transportation with optimal tip angles of 15° for $L = 1$ mm and 10° for $L = 1.5$ mm, respectively (Figure 3c). By careful consideration of both the

water condensation and transportation, the tip angle and height of the cactus-mimetic spine studied in the following experiments was 10° and 1.5 mm, respectively. We placed the spines with the optimized apex angle and height at multiple tilting angles (90°, 0°, and 45°) to determine the effects of the spine's growing direction on the directional movement behavior of the condensed water drops (Figure 3d). For each case, even when the spine was vertically fixed with the tip pointing down, the water drops were directionally driven from the tip to the base side of the spine (red arrows in Figure 3d and Movie S1, Supporting Information). These results indicate that the gravitational force of the water drop has little effect on the directional water collection performance.

As shown in Figure 3d, the tiny water drops initially deposit randomly on the 3D-printed spine surfaces (a2 and b2). As the deposition continues, water drops move toward the base of the spines due to their size increasing (a2, b2), which refreshes the original deposition sites. As soon as the newborn surface forms, another tiny water drop (b2′) appears at the same location as the former drop (b2). The next cycle of "fog deposition–drop directional movement–water collection" begins. The microscope images of the titled spines for 90° and 135° shows similar water collection phenomena. The collection on the surface with tetragonally arranged spines behaves similarly, experiencing the same fog deposition, directional drop movement, and incessant water collection (Movie S2, Supporting Information). There are two different modes in water drops directional movement with the same gradient of Laplace pressure: water drops on the surface of spines can move directly toward the base of the spines as their size is growing large enough to overcome the resistance from contact angle hysteresis,[19] such as drop c1, drop c2 in Figure 3d, or they may merge with adjacent drops first and then move directionally, similar to drop c1 and c2.[47] The second case is more favorable for driving water droplet to move due to the energy feed upon drops coalescence, which will help the merged droplets to overcome the energy barrier arising from contact angle hysteresis against the drop movement.[16] In the present work, during the fogging process, the fusion of the tiny droplets could release their surface energy, which favored the motion of the water droplet, namely, a "fusion" and "motion" process (Figure 3d).[1]

Previous studies for water collection substrates and devices were focused on the single artificial spine array due to the limitation of their manufacturing capability. However, cactus-mimetic multibranched spines can significantly improve water collection efficiency. Benefited from the ISA-3DP process, the surfaces covered with tetragonally arranged cluster array, which had a different number of spinous branches, were designed and fabricated. The water collection of the 3D-printed surfaces was quantitatively studied, and the mass gain of each surface was compared for the duration of 4 min (**Figure 4**a). When the fog flow was guided in the vertical

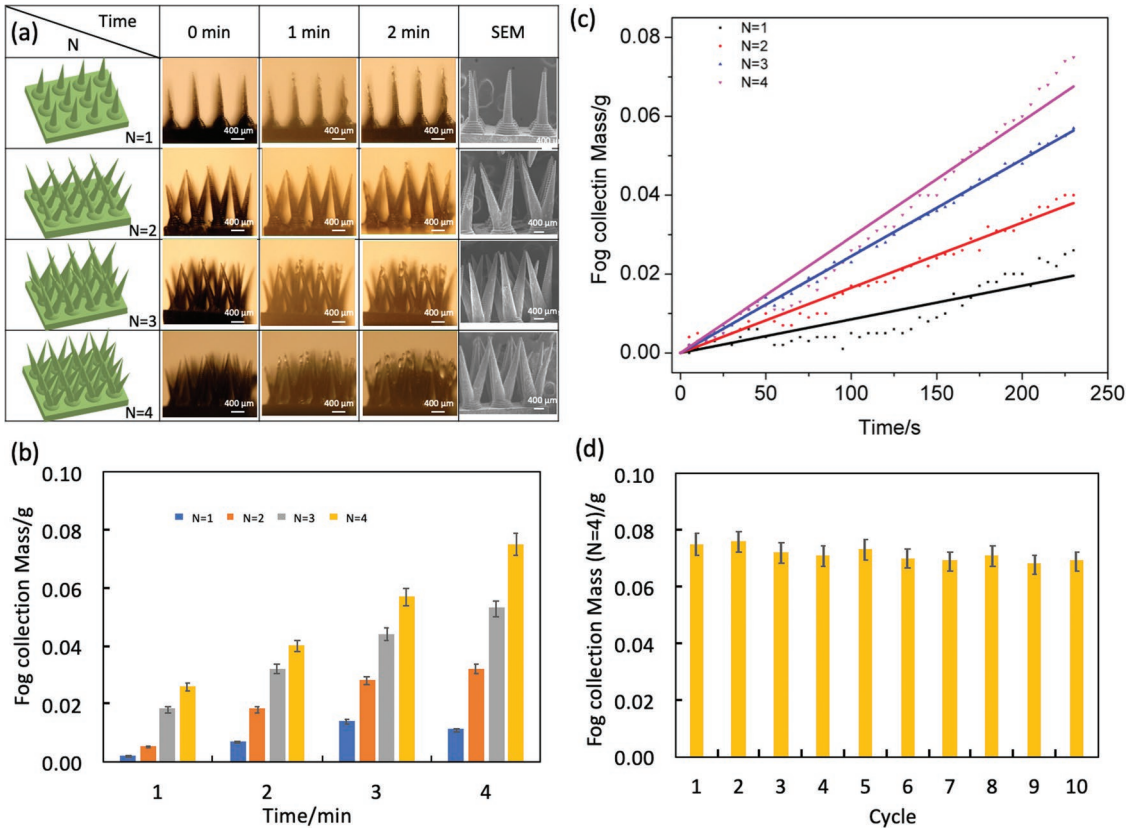

Figure 4. Water collection of 3D-printed surface decorated with multiple branched spines structures: a) microscope images of water collection process with time for different number of branched spines structures; b) the collected water masses for different number of branched spines structures at 1, 2, 3, and 4 min; c) the collected water masses for different number of branched spines structures with time; and d) changes of the collected water masses with different cycles.

direction, the clusters array with multiple branched spines promotes interception possibility per unit area of fog flow at the collector surface, resulting in high water collection efficiency. The mass of collected water on the surface decorated with four branched clusters array was four times that of the array with the single spine (Figure 4b,c).

For the 3D-printed surfaces decorated with four branched artificial spines, the collected water firstly gathered at the place where branched spines converged after 4 min, and the gathered water flew out and fed into the adjacent area between the clusters until the volume of the gathered water reached the threshold. The water in the adjacent region gradually covered all the branched spines, preventing the artificial spines to continue water collection (Figure S5, Supporting Information). The collected water was sucked out manually from the printed surface to ensure the 3D-printed artificial spines to continuously collect water from humidity flow. The recycle efficiency was tested after repeating the process for ten cycles (Figure 4d). Since the cactus-mimetic spine can be placed from different angles because of the printing capability of ISA-3DP, the water collection efficiency of cactus-mimetic spine designed with different branch angles was further studied (see Figure S6, Supporting Information). The comparison shows the branch angle of the cactus-mimetic spine had no significant influence on the water collection efficiency (see Figure S6, Supporting Information).

Even though the multiple branched spines structures can be placed in different angles, the water collection of multiple branched spines structures is closely related to the arrangement of the cactus-mimetic spine due to the airflow in various directions. Water collection occurs when tiny water drops with the diameter ranging from 8 to 40 μm contained in a fog flow are intercepted by the obstacle forward.[52] Ideally, the tiny water drops will advance with the fog flow. Given the fog flow, when it gets close to the obstacle, the part that falls to the boundary of the obstacle's projection plane is inevitably deflected due to the resistance force and continues to flow downstream. The experimental results (Figure S7, Supporting Information) demonstrate that the flow from the vertical direction uniformly surrounded the surface of tetragonally arranged spines, and the water droplet condensed at the tip of each spines. However, when the angle of fog flow was changed from the vertical to horizontal directions, the water droplet only appeared mostly on the windward side of the 3D-printed spines. The previous study showed that the flow field or the flow stream in visual representation around a fog collector is crucial to the ultimate water collection efficiency.[47]

To quantitatively display the arrangement of multibranched spines on a 3D-printed surface in collecting water, four kinds of surfaces, including the original surface (original), surface with rotation of multibranched spines (optimized 1), surface with the movement of multibranched spines (optimized 2), surface with the rotation and movement of multibranched spines (optimized 3), were placed in the same fog flow and their mass changes along the deposition time is plotted. As shown in **Figure 5**a, in the time range from 0 to 240 s, the surface with the optimized 3 structure collects the water in high efficiency. In detail, the mass of collected water on the surfaces of optimized 3, optimized 2, and optimized 1 is about 5 times, 3.5 times, and 2 times than that of the original surface, respectively. The differences arise from the different fog flow fields, and directional movement of water drops on the structured surfaces with multibranched spines. In our 3D-printed multibranched spine arrays, different arrangement will induce turbulence of the flow stream in favor of water collection. The effects of the arrangement of multibranched spine arrays by titling and movement of the multibranched spines on the flow stream were simulated and the flow stream around each branched spine is shown in Figure 5c–f. In the tetragonally arranged spines, the flow speed around the branched spines varies in different places, since the flow stream was blocked by the branched spines array in the windward side (Figure 5c and Figure S8a, Supporting Information). The conditions of flow stream around each branched spine improved when clusters of multibranched spines were arranged hexagonally (Figure 5e and Figure S8d, Supporting Information), and the flow stream was uniformly distributed among each branched spine after the position of branched spines was adjusted in case of mutual interference (Figure 5f). Based on the flow stream study of the multibranched spines arrays with the arrangement shown in optimized 3 achieved the most efficient water collection in unit volume (Movie S3, Supporting Information). For a water collection device design, different arrangements of multibranched spines arrays can be easily designed and fabricated using the ISA-3DP, and the device can be easily scaled up for large-area water collection due to its high-efficiency and low-cost printing approach. Structures with branched spines that are optimally distributed in 3D space may be studied to improve the water collection efficiency further in the future.

3. Conclusion

In conclusion, we have demonstrated the fabrication of the cactus-inspired and multibranched spines by the 3D printing process. By designing the spines with different arrangements, the 3D-printed multibranched spines with hydrophobic nanocoating and optimized tip angle shows obvious advantages compared to other structured surfaces. The underlying mechanism has three aspects: first, the more turbulent and complicated flow field around the optimized spines increases the effective deposition area, facilitating more tiny water drops' deposition and the ultimate water collection; second, directional movement of water drops on these surfaces heavily affects their water collection efficiency. Specifically, water drops on a spine-structured object feel different Laplace pressure in the two opposite sides, and the tip angle of cactus-inspired spine was optimized based on its length for fast water transportation along the spine; third, the directional transport of the collected water drops on the hydrophobic nanocoating surface benefits the quick rebirth of the deposition sites, and further favors efficient water collection. Together with the fabrication capability easy control and large-area production of 3D printing, this optimized bioinspired design opens up a new avenue to collect water with no external energy input and may be potentially useful for relieving the water crisis in arid regions.[53]

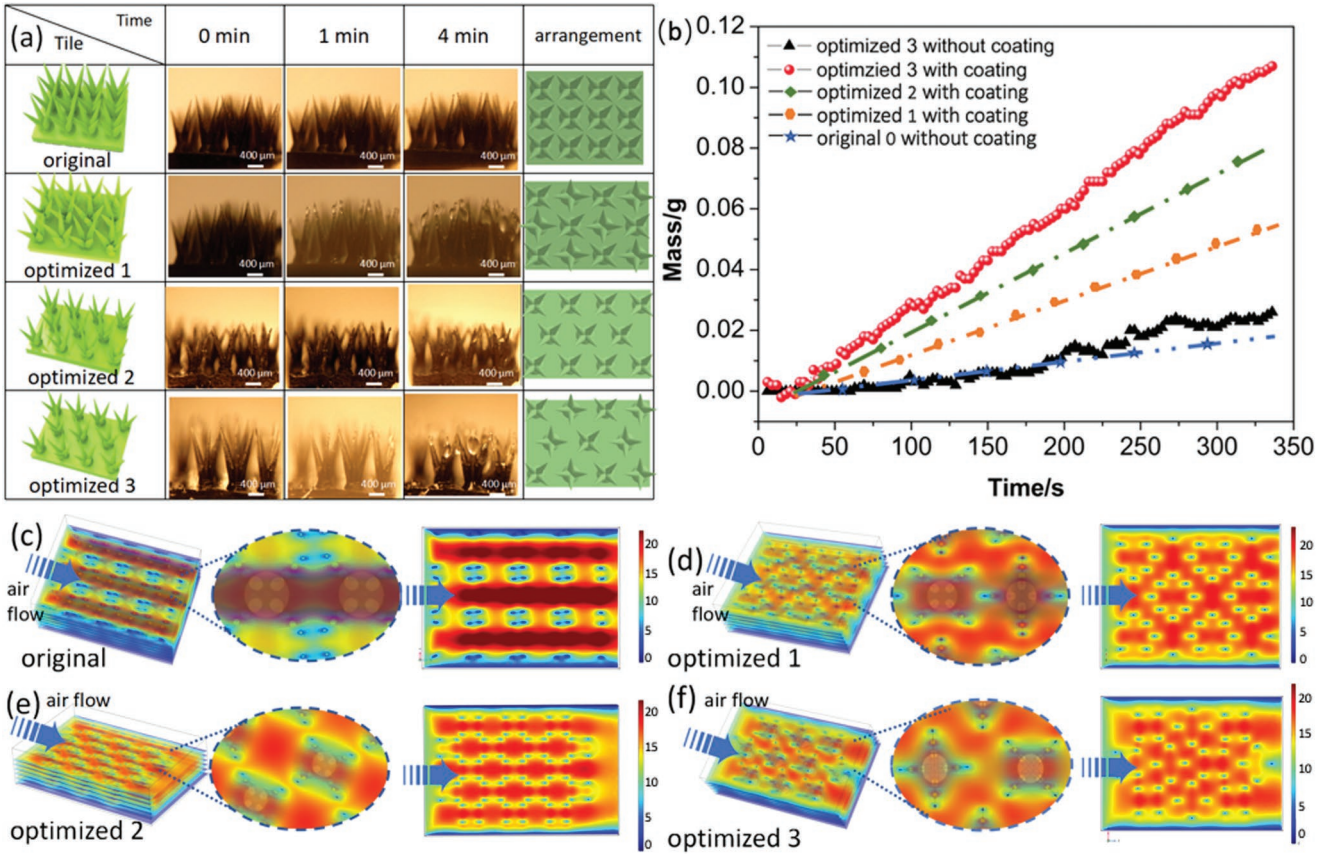

Figure 5. Water collection of the 3D-printed cactus-mimetic spine structures: a) microscope images of the water collection process over time for different arrangements of multibranched spines at 0, 1, and 4 min; b) the collected water masses for different arrangements of multibranched spines over time; and c–f) the simulation results of the fog flow around multibranched spines with different arrangements.

4. Experimental Section

Preparation of Polymer/MWCNTs Composite Resin: The photocurable polymer (E-glass) used in this study was purchased from EnvisionTEC (Dearborn, MI). The E-glass was transparent, and Oil Red O dye (purchased from Sigma-Ardrich) as visible light absorber was used at a concentration of 0.02 wt% to reduce the light penetration of E-glass resin. The Oil Red O dye was firstly mixed with E-glass resin for 1 h under magnetic stirring and then ultrasonic bath until the Oil Red O dye fully dissolved in the E-glass resin. The composite photocurable resin was prepared by mixing MWCNTS with photocurable E-glass resin. The MWCNTs (length (1–5 μm) and outer diameter (5–15 nm), from Bucky USA, Inc.) was used as it was received. It was mixed with E-glass resin for 2 h under magnetic stirring and then ultrasonic bath for 30 min. Both the polymer resin and the composite photocurable resin were degassed in the vacuum before fabrication.

ISA-3DP: ISA-3DP extended the idea of the point-based CNC accumulation process.[54] The light tool was immersed inside the resin tank, and the material was accumulated along with the moving of the light tool. The ISA-3DP system was composed of an optical system, a motion system, and a vision system.[46] Unlike the single LED dot in the point-based CNC process, the light tool in the ISA-3DP system can project 2D patterned light beam, of which the resolution was 2.5 μm pixel^{-1}. To generate the 2D patterned light beam, a digital micromirror device (DMD) based microscale optical system was designed and constructed (refer to Figure 1c). In the optical system, the visible light firstly passed through a fluorescence imaging filter (purchased from Thorlabs, Inc.) that only the 405 nm wavelength light can be transmitted. The light was reflected by DMD into the collimating lens (an achromatic doublet lens purchased from Thorlabs Inc.), making the pixel appear bright in the final 2D patterned light beam. The brightness of each pixel in the 2D patterned light beam can be controlled by adjusting the on and off frequency of each corresponding micromirror in the DMD chip. Finally, the 2D patterned light beam was generated on the top surface of the light guide tool after the collimated light was focused by 4× Olympus plan achromatic objective lens with a focus distance $f = 15$ mm (purchased from Thorlabs Inc.). The light guide tool was mounted inside the resin tank, and the inserted object was integrated with multiaxis movements so that the microscale multibranched spines can be deposited from different surface orientations.

Surface Wettability Modification: Optimizing the water collection performance of artificial spine array requires the surface wettability of the artificial spine structures to be controlled. The material used to fabricate the artificial spine arrays showed the hydrophilic property. The sample was coated with self-assembled monolayer using a vapor-phase process to improve the hydrophobicity of artificial spine arrays. In the vapor-phase process, the sample was loaded into a glassware vacuum chamber with 0.1 mL of a liquid treatment agent. Next, the chamber was pumped to 10^{-3} Torr for the treatment agent to evaporate into the vapor phase. After 10 min, the valve to the pump was closed, and the chamber held vacuum for 6 h to finish the treatment. The thickness of the coating was less than 10 nm, which made no significant impact on the surface roughness, and more details can be found in ref. [51].

Water Collection Testing and Measurement: In the water collection qualitative testing, the 3D-printed artificial spine array was mounted on the glass slide, and the glass slide was placed in an open environment, where the temperature was maintained at 23 °C. A constant velocity of fog flow generated by an ultrasonic humidifier (ASOM ultrasonic humidifier) continuously blow the 3D-printed artificial spine array from the vertical or horizontal directions and the relative humidity of

the 3D-printed artificial spine array was kept at 95%. To quantitatively measure the water collection performance, the glass slide with and without 3D-printed spine array was placed inside the analytical balances (the resolution is 1 mg), respectively (Figure S9, Supporting Information). A constant fog flow generated by the ultrasonic humidifier continuously blow from the relative direction of the analytical balances to keep the inside relative humidity at 95%. The incremental mass value of the glass slide with and without 3D-printed artificial spine array was recorded, respectively, and the difference between them was the mass of the water collected by the 3D-printed spines array. The experiment design followed the principle of statistical analysis theory, and at each time, three 3D-printed samples with the same design were measured to reduce the measurement error.

Characterization of 3D-Printed Spine Array: The water collection behavior of the 3D-printed spine array was recorded by Celestron digital microscope. The microstructures of the 3D-printed spine array were observed by an optical microscope (OMAX 40 × –2500 × LED biological microscope) and a scanning electron microscope (JEOL, JSM-7001, Japan) at the accelerating voltage of 5 kV.

Simulation by COMSOL Multiphysics: The water collection efficiency of the multibranched spine array depends on the velocity of fog flow around each spine. The velocity of the fog flow around the multibranched spine array with different arrangements was simulated by COMSOL Multiphysics software. Firstly, the 3D model of multibranched spine array with the different arrangement was designed by Solidworks and then was imported into Comsol Multiphysics. The material of flow was chosen as water vapor to simulate air with high humidity in the real environment. The multibranched spine array was placed inside a rectangular block with the boundary condition, and the boundary was defined on each face of the block as inlet, outlet, and walls so that the air flows in the horizontal direction through each artificial spine. The water vapor flow was set as a laminar flow with 10 m s^{-1}, and then the related meshes were created for the simulation. The fluid-velocity profile was generated for each multibranched spine array with a different arrangement to observe the velocity distribution of the fog flow around the multibranched spines.

Supporting Information

Supporting Information is available from the Wiley Online Library or from the author.

Acknowledgements

This work was partially supported by the National Science Foundation (NSF) Grant No. 1151191. The authors also thank Prof. Wei Wu and Dr. Yuanrui Li, for their help with the vapor-phase process. The authors also acknowledge the Core Center of Excellence in Nano Imaging at USC for the use of the microscopic measuring equipment.

Conflict of Interest

The authors declare no conflict of interest.

Keywords

additive manufacturing, biomimic material, cactus, multibranched spines, water collection

Received: October 15, 2019
Revised: November 12, 2019
Published online: December 17, 2019

[1] M. Cao, J. Ju, K. Li, S. Dou, K. Liu, L. Jiang, *Adv. Funct. Mater.* **2014**, *24*, 3235.
[2] O. Klemm, R. S. Schemenauer, A. Lummerich, P. Cereceda, V. Marzol, D. Corell, J. Van Heerden, D. Reinhard, T. Gherezghiher, J. Olivier, P. Osses, *Ambio* **2012**, *41*, 221.
[3] A. R. Parker, C. R. Lawrence, *Nature* **2001**, *414*, 33.
[4] Y. Zheng, H. Bai, Z. Huang, X. Tian, F. Nie, Y. Zhao, J. Zhai, L. Jiang, *Nature* **2010**, *463*, 640.
[5] J. Ju, H. Bai, Y. Zheng, T. Zhao, R. Fang, L. Jiang, *Nat. Commun.* **2012**, *3*, 1247.
[6] K. Yin, H. Du, X. Dong, C. Wang, J. A. Duan, J. He, *Nanoscale* **2017**, *9*, 14620.
[7] T. Nørgaard, M. Dacke, *Front. Zool.* **2010**, *7*, 23.
[8] E. J. Edwards, M. J. Donoghue, *Am. Nat.* **2006**, *167*, 777.
[9] R. M. Ogburn, E. J. Edwards, *Am. J. Bot.* **2009**, *96*, 391.
[10] M. E. Loik, *Physiol. Plant.* **2008**, *134*, 87.
[11] H. A. Mooney, S. L. Gulmon, P. J. Weisser, *Flora* **1977**, *166*, 117.
[12] A. Mosco, *Rev. Mex. Biodiver.* **2009**, *80*, 119.
[13] R. Schill, W. Barthlott, N. Ehler, *Cactus Succulent J.* **1973**.
[14] J. D. Mauseth, *Ann. Bot.* **2006**, *98*, 901.
[15] M. K. Chaudhury, G. M. Whitesides, *Science* **1992**, *256*, 1539.
[16] S. Daniel, M. K. Chaudhury, J. C. Chen, *Science* **2001**, *291*, 633.
[17] É. Lorenceau, D. Quéré, *J. Fluid Mech.* **2004**, *510*, 29.
[18] P. Renvoisé, J. W. Bush, M. Prakash, D. Quéré, *EPL* **2009**, *86*, 64003.
[19] H. Bai, X. Tian, Y. Zheng, J. Ju, Y. Zhao, L. Jiang, *Adv. Mater.* **2010**, *22*, 5521.
[20] L. Zhai, M. C. Berg, F. C. Cebeci, T. Kim, J. M. Milwid, M. F. Rubner, R. E. Cohen, *Nano Lett.* **2006**, *6*, 1213.
[21] R. P. Garrod, L. G. Harris, W. C. Schofield, J. McGettrick, L. J. Ward, D. O. Teare, J. P. Badyal, *Langmuir* **2007**, *23*, 689.
[22] C. Dorrer, J. Rühe, *Langmuir* **2008**, *24*, 6154.
[23] S. C. Thickett, C. Neto, A. T. Harris, *Adv. Mater.* **2011**, *23*, 3718.
[24] J. Ju, K. Xiao, X. Yao, H. Bai, L. Jiang, *Adv. Mater.* **2013**, *25*, 5937.
[25] J. Zhang, Y. Han, *Langmuir* **2007**, *23*, 6136.
[26] C. Sun, X. W. Zhao, Y. H. Han, Z. Z. Gu, *Thin Solid Films* **2008**, *516*, 4059.
[27] G. Fang, W. Li, X. Wang, G. Qiao, *Langmuir* **2008**, *24*, 11651.
[28] J. T. Yang, Z. H. Yang, C. Y. Chen, D. J. Yao, *Langmuir* **2008**, *24*, 9889.
[29] S. J. Moon, S. S. Lee, H. S. Lee, T. H. Kwon, *Microsyst. Technol.* **2005**, *11*, 311.
[30] S. P. Sullivan, N. Murthy, M. R. Prausnitz, *Adv. Mater.* **2008**, *20*, 933.
[31] K. Li, J. Ju, Z. Xue, J. Ma, L. Feng, S. Gao, L. Jiang, *Nat. Commun.* **2013**, *4*, 2276.
[32] K. A. Moga, L. R. Bickford, R. D. Geil, S. S. Dunn, A. A. Pandya, Y. Wang, J. H. Fain, C. F. Archuleta, A. T. O'Neill, J. M. DeSimone, *Adv. Mater.* **2013**, *25*, 5060.
[33] H. Zhu, Z. Guo, W. Liu, *Chem. Commun.* **2016**, *52*, 3863.
[34] X. Heng, M. Xiang, Z. Lu, C. Luo, *ACS Appl. Mater. Interfaces* **2014**, *6*, 8032.
[35] H. Cho, B. Park, M. Kim, S. Lee, W. Hwang, *J. Mater. Chem. A* **2017**, *5*, 25328.
[36] Y. S. Leung, T. H. Kwok, X. Li, Y. Yang, C. C. Wang, Y. Chen, *J. Comput. Inf. Sci. Eng.* **2019**, *19*, 021013.
[37] Y. Yang, X. Song, X. Li, Z. Chen, C. Zhou, Q. Zhou, Y. Chen, *Adv. Mater.* **2018**, *30*, 1706539.
[38] Y. Yang, X. Li, X. Zheng, Z. Chen, Q. Zhou, Y. Chen, *Adv. Mater.* **2018**, *30*, 1704912.
[39] Y. Yang, X. Li, M. Chu, H. Sun, J. Jin, K. Yu, Q. Wang, Q. Zhou, Y. Chen, *Sci. Adv.* **2019**, *5*, eaau9490.
[40] X. Li, Y. Yang, B. Xie, M. Chu, H. Sun, S. Hao, Y. Chen, Y. Chen, *Adv. Mater. Technol.* **2019**, *4*, 1800476.
[41] K. C. Park, P. Kim, A. Grinthal, N. He, D. Fox, J. C. Weaver, J. Aizenberg, *Nature* **2016**, *531*, 78.
[42] C. Liu, Y. Xue, Y. Chen, Y. Zheng, *Sci. Rep.* **2015**, *5*, 17757.
[43] J. Ju, Y. Zheng, L. Jiang, *Acc. Chem. Res.* **2014**, *47*, 2342.

[44] H. Bai, J. Ju, Y. Zheng, L. Jiang, *Adv. Mater.* **2012**, *24*, 2786.
[45] B. S. Lalia, S. Anand, K. K. Varanasi, R. Hashaikeh, *Langmuir* **2013**, *29*, 13081.
[46] X. Li, Y. Chen, *J. Manuf. Processes* **2017**, *28*, 531.
[47] J. Ju, X. Yao, S. Yang, L. Wang, R. Sun, Y. He, L. Jiang, *Adv. Funct. Mater.* **2014**, *24*, 6933.
[48] L. R. Fisher, R. A. Gamble, J. Middlehurst, *Nature* **1981**, *290*, 575.
[49] M. Cao, J. Xiao, C. Yu, K. Li, L. Jiang, *Small* **2015**, *11*, 4379.
[50] X. Dai, N. Sun, S. O. Nielsen, B. B. Stogin, J. Wang, S. Yang, T. S. Wong, *Sci. Adv.* **2018**, *4*, eaaq0919.
[51] G. Y. Jung, Z. Li, W. Wu, Y. Chen, D. L. Olynick, S. Y. Wang, W. M. Tong, R. S. Williams, *Langmuir* **2005**, *21*, 1158.
[52] C. Martorell, E. Ezcurra, *Oecologia* **2007**, *151*, 561.
[53] S. Zhang, J. Huang, Z. Chen, Y. Lai, *Small* **2017**, *13*, 1602992.
[54] D. Bourell, B. Stucker, Y. Chen, C. Zhou, J. Lao, *Rapid Prototyping J.* **2011**, *17*, 218.

